

Chirped Pulse Analysis and Control in Non-Hermitian Scattering Systems using Complex Time Delay

ISABELLA L. GIOVANNELLI,^{1,*} STEVEN M. ANLAGE,¹ AND THOMAS M. ANTONSEN²

¹*Quantum Materials Center, Department of Physics University of Maryland, College Park, Maryland 20742, USA*

²*Department of Electrical and Computer Engineering University of Maryland, College Park, Maryland, 20742, USA*

*igiovann@umd.edu

Abstract: We theoretically and experimentally establish a connection between linearly chirped pulse propagation properties and complex time delay for both transmitted and reflected pulses in reverberant scattering systems. We demonstrate that the time shift of the chirped pulse depends on both the real and imaginary parts of the complex time delay of the scattering system. We also show that the chirped pulse experiences a center frequency shift that is directly proportional to the imaginary component of complex time delay, similar to that found in Ref. [1]. Using these insights, we then demonstrate how complex time delay can be harnessed to systematically tune the propagation properties of a chirped pulse such that a near-zero time shift can be achieved for a wide range of pulse center frequencies in a resonant scattering system.

1. Introduction

Chirped pulses are pulses whose instantaneous frequency varies throughout the pulse. They are the basis for multiple modern technologies and are present in various physical phenomena. A nonexhaustive list includes chirped pulse amplification [2]; chirped pulse interferometry [3, 4] and spectroscopy [5]; lidar, radar, and sonar [6–11]; fiber optics and photonics [7, 12–15]; frequency domain reflectometry [8, 16]; attosecond pulse control [17–19]; qubit control [20–22]; digital computing [16]; wireless communication [23, 24] and biological/medical imaging [25–29]. Chirped pulses are widely utilized for their ability to be compressed and expanded without altering their frequency bandwidth. This allows for ultrashort intense pulses to be safely amplified without changing their spectrum. This also allows for the creation of long pulses with large frequency bandwidths which then provide long range high resolution measurements that are robust against dispersion. These advantages are what have made chirped pulses so versatile. In all these applications, it is imperative to have precise control over the propagation of a chirped pulse through a given scattering environment, particularly its time delay.

In this paper we focus on understanding and controlling the time delay of linearly chirped pulses. In particular we are concerned with *linear* pulse propagation through a non-Hermitian dispersive system where the incident waves can be related to the output waves via the transmission or reflection matrix [30, 31]. They are sub-matrices (or coefficients if $M \leq 2$) of the $M \times M$ scattering matrix (S) where M is the total number of scattering channels.

In this paper we use an extension of Wigner-Smith time delay [32–34] to describe how long a wave lingers in a non-Hermitian scattering system. Wigner-Smith time delay was originally defined in the context of unitary nuclear scattering as $\tau_W(E) = -\frac{i}{M} \frac{d}{dE} \ln[\det S(E)]$ where E is energy. This concept was later generalized to include non-unitary dispersive scattering systems in the context of classical electromagnetic waves [31, 35]. We use this extension, referred to as complex time delay (CTD), to define the time delay of a chirped electromagnetic pulse as it travels through a resonant scattering system. CTD is expressed as,

$$\tau = \frac{-i}{2\pi} \frac{\partial}{\partial f} \ln[\rho(f)] = \text{Re}[\tau] + i\text{Im}[\tau] \quad (1)$$

where τ is transmission/reflection time delay, ρ is the scattering matrix transmission/reflection coefficient, and f is frequency. This generalization of time delay is complex due to the sub-unitary and dispersive nature of the matrix elements [31, 35]. This can be seen by representing complex $\rho(f)$ in terms of a frequency dependent magnitude and phase. The real and imaginary parts of these delays can be positive, negative or zero.

There has been considerable effort to understand the physical meaning behind negative real time delay, or fast light, measured with Gaussian pulses [36–41]. This phenomenon occurs when the group velocity of light is either greater than the speed of light in vacuum, or negative. This happens, for example, in systems near/at a resonance where there is a large amount of anomalous dispersion [39]. These cases have been observed experimentally [40, 42] and are both interpreted as the result of extreme nonuniform attenuation of the Fourier components of the pulse as it travels through the anomalously dispersive medium. Note that the general pulse shape is not distorted as long as the frequency bandwidth of the pulse is less than the width of the resonance being excited in the system [36, 39]. The nonuniform change in the Fourier components leads to a shift in time of the pulse peak, creating the illusion that the pulse has left the system before it has entered [37, 39]. This does not violate causality since there is a distinction between group velocity and information velocity as explained by Sommerfeld and Brillouin [43–45] and experimentally demonstrated in Ref. [42]. There has also been recent work on interpreting negative time delay in quantum mechanical systems, where in Refs. [46, 47] they explore the time delay of a photon traveling through an atom cloud.

Imaginary time delay has received considerably less attention than negative time delay/fast light. Imaginary transmission time delay was first properly predicted to correspond to a center frequency shift in a Gaussian pulse in Ref. [48], and experimentally confirmed in Ref. [1]. Imaginary time delay occurs for the same reason that negative time delay does: it is the result of nonuniform distortion of the Fourier components as the pulse travels through an anomalously dispersive linear medium.

We now wish to generalize the complex time delay results presented in Refs. [1, 48] to chirped pulses, which are of great interest to many different fields and applications. Here we theoretically and experimentally demonstrate how properties of a chirped pulse change as it travels through a linear dispersive scattering system. We also show how these changes in pulse properties can be accurately predicted with only knowledge of the complex transmission (or reflection) coefficient as a function of frequency. Specifically, we analyze how the peak of the chirped pulse shifts in time as well as how its center frequency changes. We confirm that the frequency shifts are directly proportional to imaginary time delay in a manner similar to that shown in Refs. [1, 48]. We also show that the peak time shifts of a chirped pulse depend not only on the real part of complex time delay but also in a non-trivial way on the imaginary part.

2. Chirped pulse properties and complex time delay

The predicted results connecting complex time delay and chirped pulse properties can be derived following a similar process demonstrated in Refs. [1, 48, 49]. The details for this calculation can be found in the supplementary materials. We define a linearly chirped pulse to be the following:

$$E_i(t) \propto \exp \left[-i2\pi f_0 t - (i\Omega' + \delta_t^{-2}) \frac{t^2}{2} \right] \quad (2)$$

where f_0 is the center frequency of the pulse, Ω' is the chirp rate and $\delta_t = \frac{\delta_T}{2\sqrt{2\ln 2}}$ where δ_T is the full width at half maximum of the amplitude of the pulse in the time domain. The frequency

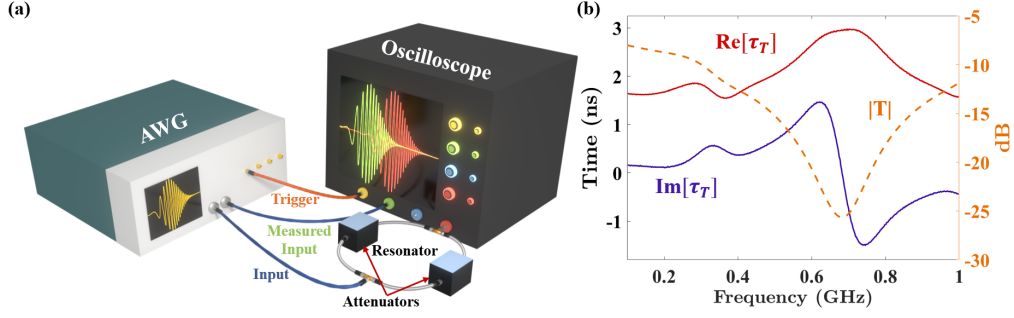


Fig. 1. (a) Schematic of time domain experiment setup. The ring resonator depicted is the one that was used for the transmission case. (b) Complex time delays and transmission magnitude (in dashed orange) for the resonator depicted in (a). The red and dark purple solid lines respectively correspond to the real and imaginary parts of transmission time delay (τ_T).

bandwidth of the chirped pulse is subsequently defined as,

$$\delta_f = \frac{1}{\pi} \sqrt{2 \ln 2 (\Omega'^2 \delta_t^2 + \delta_t^{-2})} \quad (3)$$

where δ_f is the FWHM of the chirped pulse amplitude in the frequency domain in Hz. Note that in this formulation of a chirped Gaussian pulse, the chirp rate is bounded by the chosen frequency bandwidth of the pulse,

$$\Omega' \leq \frac{(\pi \delta_f)^2}{4 \ln 2} \quad (4)$$

The explanation for this bound is contained in section B of the supplementary materials.

We consider the case of a pulse propagating through a linear dispersive system for which the pulse frequency bandwidth (Eq. (3)) is much smaller than the 3 dB linewidth of the chosen resonance of the scattering system. Note that we treat the scattering system in terms of its dispersive overall transmission/reflection coefficient, rather than as a continuous extended medium in space. We define the shifts in frequency and time to be the shifts in frequency of the peak of the power spectral density, and shifts in time of the peak of the pulse power, respectively. These are directly related to the CTD of the scattering system. The shift in center frequency is predicted to be,

$$D_f = -\tilde{\Delta}^2 \text{Im}[\tau] \quad (5)$$

where D_f is the shift in center frequency in Hz and $\tilde{\Delta} = \frac{1}{2\pi} \sqrt{\Omega'^2 \delta_t^2 + \delta_t^{-2}} = \frac{\delta_f}{2\sqrt{2 \ln 2}}$ is proportional to the bandwidth of the chirped pulse. The time shift in the output pulse is found to be,

$$D_t = \text{Re}[\tau] - \Omega' \delta_t^2 \text{Im}[\tau] \quad (6)$$

where D_t is the predicted time shift of the chirped pulse which, surprisingly, depends on the imaginary part of time delay, in addition to the real part, weighted by a factor of the chirp-duration product $\Omega' \delta_t^2$. This allows for an extraordinary degree of control of D_t , as demonstrated in Fig. 5, where we achieve the $D_t = 0$ condition over a broad range of pulse center frequencies.

3. Experiment

The time domain experiment setup is depicted in Fig. 1(a), where we use a signal generator to create a chirped pulse that is sent through the resonant system and then measured on an

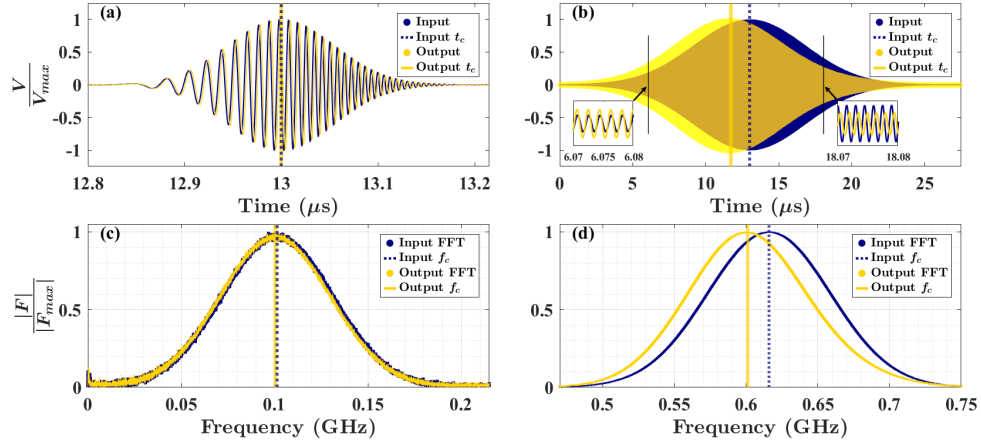


Fig. 2. Examples of the normalized chirped pulses sent through the resonator depicted in Fig. 1(a). The pulses sent into the resonator are plotted in blue and the output pulses are plotted in yellow. The measured center frequencies (f_c) and transmission times (t_c) are shown as corresponding vertical lines. The insets in (b) show detailed oscillations of the pulses in equal-width (10 ns) time windows, illustrating the chirped nature of the pulse.

oscilloscope. In more detail, a chirped pulse is produced using a 50 GSa/s Tektronix model AWG70001B arbitrary waveform generator (AWG). The time domain expression used to define the chirped pulse is given by the imaginary part of Eq. (2). The two output ports on the AWG (1+, 1-) produce nominally identical pulses that are sent through twin 33.02 cm-long coaxial cables. Port 1- is connected directly to channel 2 of a Keysight/Infiniium model UXR0104A 25-GHz bandwidth real-time digital sampling oscilloscope (DSO), which captures the "measured input pulse". Port 1+ of the AWG is connected to the resonator. The output pulse from the resonator is then measured on channel 4 of the oscilloscope. Lastly, the orange cable connects the AWG marker channel (M1+) to channel 1 of the oscilloscope and acts as the trigger signal. We note that Port 1- is the differential complement of Port 1+. The pulses coming out of these ports need to be identical in order to have a valid comparison between the pulse that travels through the "measured input cable" and the pulse that travels through the whole system. We meet this condition by simply multiplying the output signal from Port 1- by -1.

In a separate experiment, the complex transmission $T(f)$ and reflection $R(f)$ coefficients of the ring resonator were measured using a Keysight N5242A network analyzer (PNA-X) that is calibrated using a Keysight N4691-60001 Electronic Calibration kit at the resonator's connection points. The measured transmission coefficient magnitude shown in Fig. 1(b) is taken over the frequency range 0.1 GHz to 1 GHz with a frequency step size of 1.331 MHz. The reflection coefficient magnitude shown in Fig. 4(b) was measured over the frequency range of 1 GHz to 2 GHz with a frequency step size of 1.66 MHz. The corresponding real and imaginary parts of complex transmission and reflection time delay calculated using Eq. (1), are shown as solid lines in Figs. 1(b) and 4(b), respectively.

The transmission and reflection measurements were performed using the same experimental setup, but with two different resonators. Different resonators were used in the two cases to establish wide resonances of comparable size, which then provided similarly sized large D_t and D_f values for transmission and reflection, which are shown in Figs. 3 and 4, respectively. The transmission resonance is situated at 0.684 GHz and has a 3-dB frequency bandwidth of about 117 MHz. The reflection resonance is centered at 1.19 GHz with a 3-dB bandwidth of 82 MHz.

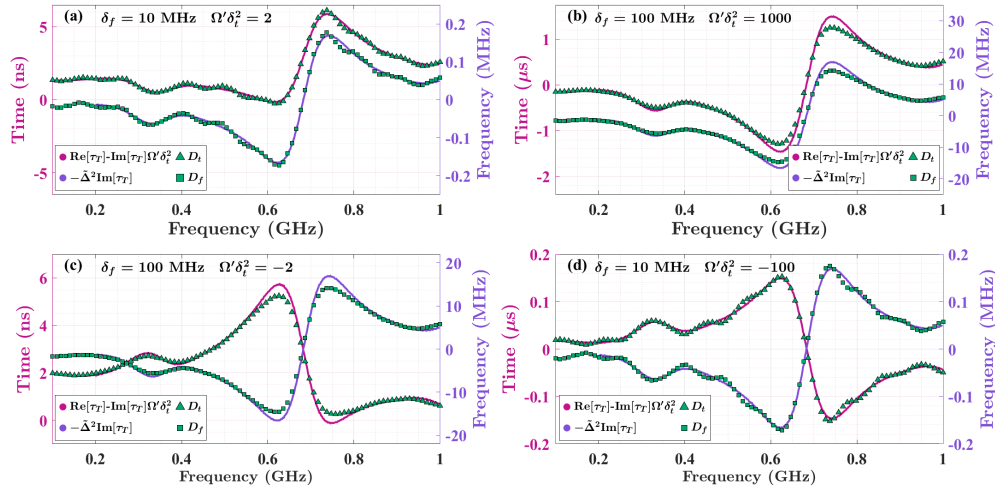


Fig. 3. Summary of measured and expected time delays and frequency shifts for chirped pulses having various $\Omega'\delta_t^2$ and δ_f values, as a function of center frequency. The predicted time shift is plotted in magenta and the measured pulse time shift are the green triangles. The predicted frequency shift is in light purple and the measured pulse frequency shift is plotted as green squares. The chirp rates and pulse widths used are as follows: (a) $\Omega' = 0.2848 \frac{\text{MHz Rad}}{\text{ns}}$ and $\delta_t = 83.8 \text{ ns}$, (b) $\Omega' = 0.0712 \frac{\text{MHz Rad}}{\text{ns}}$ and $\delta_t = 3747.82 \text{ ns}$, (c) $\Omega' = -28.48 \frac{\text{MHz Rad}}{\text{ns}}$ and $\delta_t = 8.38 \text{ ns}$, (d) $\Omega' = -0.0071 \frac{\text{MHz Rad}}{\text{ns}}$ and $\delta_t = 3748 \text{ ns}$

The resonator used in the transmission case was a microwave ring resonator [31, 50] consisting of 4 coaxial cables and 2 identical Narda (model 4745-69) step attenuators, as shown in Fig. 1(a). Two of the cables are each 15.24 cm-long and are attached to either side of a step attenuator set at 5 dB. The other two cables are each 7.62 cm-long and are attached to either side of the other step attenuator set at 9 dB. The ring is completed with two ‘tee’ junctions, creating a 2-port network.

The ring resonator used for the reflection case is depicted in Fig. 4(a). It is composed of a 1-2 GHz Pasternack model PE83CR003 microwave circulator that is connected through a ‘tee’ junction to two identical 12.7 cm-long coaxial cables forming a ring with a Narda (model 4745-69) attenuator set to 1 dB connected with a ‘tee’ junction on the other side. The opposing port on the attenuator was connected to a short circuit to encourage the wave to make a round trip through the attenuator before returning to the ring. One port of the circulator is the input, while the output was connected to a male-to-male adapter that was directly connected to the oscilloscope.

4. Data and Discussion

Figure 2 shows normalized raw transmitted pulse data of a few representative measured input and output pulses, their corresponding Fourier transforms, and the time/frequency shifts extracted from the data. The input pulses are in dark blue and the corresponding outputs are in yellow. Panels (a) and (c) of Fig. 2 correspond to a pulse with center frequency $f_c = 0.1013 \text{ GHz}$ and a chirp rate of $\Omega' = 3.39 \frac{\text{MHz Rad}}{\text{ns}}$. This pulse has a time width (δ_t) of 54.89 ns, a frequency bandwidth (δ_f) of 70 MHz, and a chirp factor ($\Omega'\delta_t^2$) of 10.20. This serves as an example of a pulse with both a minimum transmission time ($D_t = 0.10 \pm 0.03 \text{ ns}$) and a minimum center frequency shift ($D_f = -0.8479 \pm 0.0140 \text{ MHz}$). (The uncertainty estimates are detailed in the

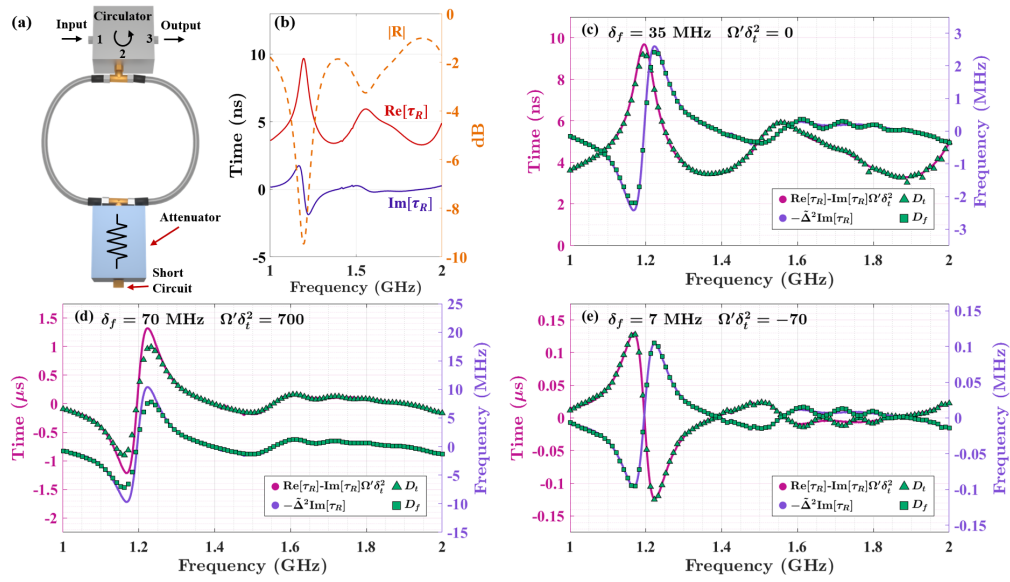


Fig. 4. (a) Schematic of reflection resonator. (b) The red and dark purple solid curves are the real and imaginary parts of reflection time delay respectively. The orange dashed curve corresponds to the magnitude of the reflection coefficient for the resonator in (a). (c-e) Summary of measured and expected time shifts and frequency shifts for chirped pulses after reflection from a ring resonator. The predicted center frequency shifts are shown in light purple, and predicted time shifts in magenta with the measured frequency shifts represented as green rectangles and time shifts represented as green triangles. This is done for various chirped pulse frequency bandwidths (δ_f) and $\Omega'\delta_t^2$ values. The chirp rates and pulse widths used are as follows: (c) $\Omega' = 0 \frac{\text{MHz Rad}}{\text{ns}}$ and $\delta_t = 10.71 \text{ ns}$, (d) $\Omega' = 0.0498 \frac{\text{MHz Rad}}{\text{ns}}$ and $\delta_t = 3747.80 \text{ ns}$, (e) $\Omega' = -0.005 \frac{\text{MHz Rad}}{\text{ns}}$ and $\delta_t = 3747.87 \text{ ns}$.

Supp. Mat.) Panels (b) and (c) of Fig. 2 correspond to a pulse from the data shown in Fig.3 (b) with a center frequency of 0.6157 GHz, which situates it right near peak resonance. The insets on either side of the pulse are zoomed-in regions of detailed oscillations to illustrate that the pulse is not just a Gaussian pulse but a chirped Gaussian pulse. The pulse has a chirp rate of $0.071 \frac{\text{MHz Rad}}{\text{ns}}$, and a pulse length (δ_t) of $3.75 \mu\text{s}$. This is an example of a pulse that undergoes both a large negative time shift ($D_t = -1.2904 \pm 0.0001 \mu\text{s}$) and a large negative frequency shift ($D_f = -14.6576 \pm 0.0006 \text{ MHz}$). The transmission times (t_c) and center frequencies (f_c) are depicted as vertical lines in Fig. 2, and are calculated using the first temporal moment of the pulse, as done in Ref. [1]. This is valid since we are working in the small bandwidth limit where the frequency bandwidth of the pulse is less than the 3-dB bandwidth of the excited resonance, hence higher-order terms in the phase and attenuation vs. frequency expressions can be neglected (see Supp. Mat. Section A). The pulse in panels (a) and (c) has a frequency bandwidth of 70 MHz, and the pulse in panels (b) and (d) has a bandwidth of 100 MHz which are both smaller than the width of the transmission resonance (117 MHz).

The main results comparing the measured time and frequency shifts with the predictions made in Eqs. 5-6 are shown in Figs. 3 and 4(c-e), for transmission and reflection, respectively. The time-domain transmission data consists of 93 data points taken over the pulse center frequency range 0.1-1 GHz and the reflection time-domain data consists of 32 data points taken over 1-2 GHz. The symbols show the time-domain D_t and D_f measurements, while the solid lines show quantities constructed from frequency-domain data to test Eqs. (5) and (6). Shown are data from

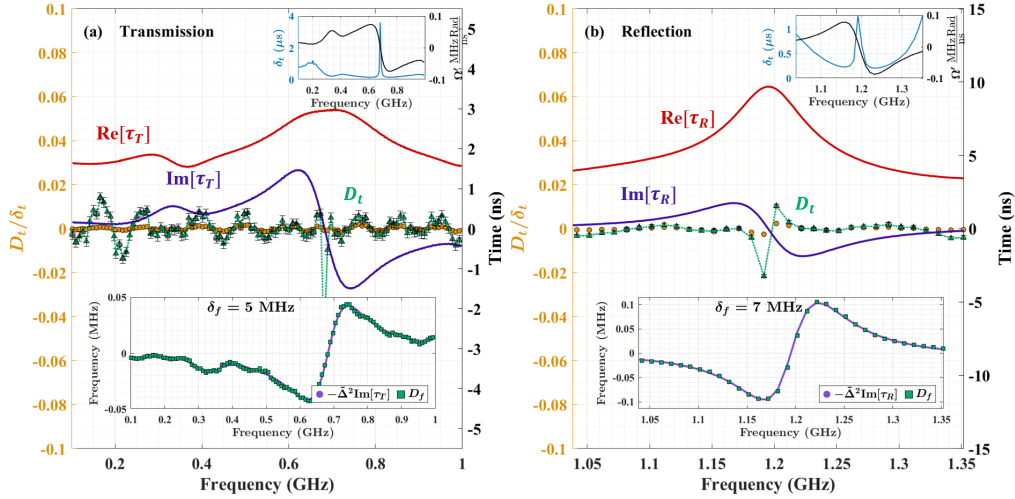


Fig. 5. Results for the case where the chirped-pulse temporal shift is canceled by setting $\text{Re}[\tau]/\text{Im}[\tau] = \Omega' \delta_f^2$ at each choice of center frequency. Panels (a) and (b) are the results for transmission and reflection, respectively. The green triangles correspond to the measured chirped pulse transmission (a) and reflection (b) time (right axis). The light orange circles correspond to time-shift normalized to the width of the pulse (left axis). The real and imaginary parts of transmission (a) and reflection (b) time delay are plotted in red and dark purple respectively. The lower insets in (a) and (b) show the predicted and measured center frequency shifts plotted in light purple and as green squares, respectively, along with the value of the common pulse bandwidth δ_f . The upper insets show the chosen values of δ_t and Ω' versus frequency utilized to achieve $D_t = 0$ for the chirped pulse.

a variety of pulses with different bandwidths δ_f and chirp rates $\Omega' \delta_f^2$ (positive and negative). From this we see that the predictions are consistent with the experimental results for a variety of pulse frequency bandwidths and chirp parameter values. We see that the frequency shifts (D_f) scale with the pulse frequency bandwidth squared, as expected from Eq. 5. We also see that there is less agreement for large frequency bandwidths as they approach the 3-dB-linewidth of the resonance being excited. This is expected as this is where the theory starts to break down (see Supp. Mat. Section A). This was the main motivation for designing resonators to have wide modes so that we could achieve such large frequency shifts. Note that the case of an un-chirped pulse is included for reflected pulses in Fig. 4(c); the un-chirped case for transmission was already experimentally demonstrated in Ref. [1] so it is omitted from this paper. Additional data for the reflection case is included in Supp. Mat. Section C.

It is clear from the data that the time shift of the pulse is heavily dependent on the magnitude of the dimensionless chirp parameter $\Omega' \delta_f^2$. We see that in both transmission and reflection, the time shift jumps from being on the scale of nanoseconds to microseconds, scaling with $\Omega' \delta_f^2$. We note that in the limit of large $\Omega' \delta_f^2$, and/or large $\text{Im}[\tau]$, D_t converges to a frequency dependence that is identical to that of D_f (modulo a sign). This makes sense when looking at Eq. 6 where the imaginary part of time delay is expected to dominate the time shift in the chirped pulse when $\Omega' \delta_f^2$ is large. This is also true for the negative chirp case, except we see that the shape of the time shift curve is reflected over the frequency axis, following the sign of the chirp rate (demonstrated in Figs. 3(d) and 4(e)).

In Fig. 5 we demonstrate how with knowledge of complex time delay one can manipulate the chirped pulse properties such that the time shift of the pulse is zero. Combining Eqs. 6

and 22 allows one to choose unique values for δ_t and Ω' , for a given bandwidth δ_f , such that $\text{Re}[\tau]/\text{Im}[\tau] = \Omega' \delta_t^2$, resulting in a zero time shift $D_t = 0$ of the chirped pulse. We tested this experimentally for both transmission and reflection, and the results are shown in Fig. 5. Shown there are $\text{Re}[\tau]$ and $\text{Im}[\tau]$ (red and blue solid lines) vs. frequency, as well as the resulting time shifts D_t (green symbols) over a broad range of pulse center frequency, for both transmission and reflection. The average D_t value over the bandwidth found for the transmission case in Fig. 5(a) is -0.03 ± 0.12 ns, which is a shift in time that is 0.0026% of the pulse width. The average D_t value found for the reflection case in Fig. 5(b) is -0.14 ± 0.12 ns or a 0.0091% temporal shift. We see that it is indeed possible to achieve $D_t = 0$ for chirped pulses over a broad range of center frequencies. We found for pulses with a frequency bandwidth around 5 MHz, that the uncertainty in the time shift is around ± 0.12 ns and the uncertainty in the calculated frequency shift is approximately ± 0.6 kHz. The error bars on the shift in time is shown in Fig. 5, whereas we do not place error bars on the frequency shift measurements because the uncertainty is smaller than the size of the data symbol.

Achieving $D_t \approx 0$ was significantly more difficult for the reflection case, where we were only able to achieve well behaved $D_t \approx 0$ behavior near resonance. When looking off resonance at the imaginary part of reflection time delay (shown in Fig. 4(b)) we see that there are multiple zero crossings and that in general the imaginary part tends to hover around zero. Since $\text{Re}[\tau]/\text{Im}[\tau] = \Omega' \delta_t^2$ we expect there to be divergences when $\text{Im}[\tau] = 0$. The full data set is located in Fig. 9 of the Supp Mat, where we see sharp increases in D_t where $\text{Im}[\tau]=0$. Additionally, see Fig. 8 in the Supp Mat where we perform this same study with pulses having 50-70 MHz frequency bandwidth.

5. Conclusion

In this paper we have established a comprehensive theoretical and experimental framework connecting complex time delay to the properties of linearly chirped pulses traveling through resonant scattering systems. Building upon the work in Refs. [1, 48], we have demonstrated that both the real and imaginary components of complex time delay play essential roles in determining chirped pulse behavior, with the imaginary part contributing not only to the observed frequency shifts but also to the temporal shifts weighted by the chirp parameter $\Omega' \delta_t^2$.

The experimental validation for both cases of transmission and reflection, spanning a wide range of chirp rates (both positive and negative) and pulse frequency bandwidths, confirms the robustness of our theoretical predictions and their practical utility. This allows one to construct chirped pulses with predetermined temporal and spectral characteristics using only knowledge of the system's transmission or reflection coefficient. This was demonstrated in Fig. 5 where we used the resonator's transmission/reflection coefficient to appropriately choose the chirp rate and pulse duration such that the time shift D_t of the pulse is nullified over a wide frequency range. The ability to achieve near-zero broadband time shifts opens new possibilities for precision control in various applications ranging from pulse compression systems to quantum computing. This result also represents a new way to take advantage of the additional degrees of freedom present in chirped pulses, going beyond what is achievable with unchirped pulses alone.

Looking ahead, there are several interesting avenues for future work. Extension to multi-mode systems with overlapping resonances would test how our theory holds in more realistic environments where mode coupling and interference effects become important. Similarly, it would be interesting to see how our theory can be expanded to systems with more than two ports or for nonlinearly chirped pulses. Additionally, since in this paper we only used simple microwave ring resonators, it would be valuable to examine how a resonator's geometry or characteristics (i.e. coupling strength, loss, Q-factor, etc.) impact the achievable range for D_t and D_f . Another open question would be how these results translate to the optical domain using systems such as an optical ring resonator or a whispering gallery mode resonator.

Funding. This work was partially supported by NSF/RINGS under grant No. ECCS-2148318, ONR under grant N000142312507, and DARPA WARDEN under grant HR00112120021.

References

1. I. L. Giovannelli and S. M. Anlage, "Physical interpretation of imaginary time delay," *Phys. Rev. Lett.* **135**, 043801 (2025).
2. D. Strickland and G. Mourou, "Compression of amplified chirped optical pulses," *Opt. Commun.* **56**, 219–221 (1985).
3. R. Kaltenbaek, J. Lavoie, D. N. Biggerstaff, and K. J. Resch, "Quantum-inspired interferometry with chirped laser pulses," *Nat. Phys.* **4**, 864–868 (2008).
4. M. M. Bérubé, M. D. Mazurek, and K. J. Resch, "Enhanced-resolution chirped-pulse interferometry," *Phys. Rev. A* **112**, 023525 (2025).
5. G. B. Park and R. W. Field, "Perspective: The first ten years of broadband chirped pulse fourier transform microwave spectroscopy," *The J. Chem. Phys.* **144**, 200901 (2016).
6. C. Allen, Y. Cobanoglu, Sekken Kenny Chong, and S. Gogineni, "Performance of a 1319 nm laser radar using RF pulse compression," *IGARSS 2001. Scanning Present. Resolv. Futur. Proceedings. IEEE 2001 Int. Geosci. Remote. Sens. Symp. (Cat. No.01CH37217)* **3**, 997–999 (2001).
7. P. Adany, C. Allen, and R. Hui, "Chirped Lidar Using Simplified Homodyne Detection," *J. Light. Technol.* **27**, 3351–3357 (2009).
8. R. E. Saperstein, N. Alic, S. Zamek, *et al.*, "Processing advantages of linear chirped fiber Bragg gratings in the time domain realization of optical frequency-domain reflectometry," *Opt. Express* **15**, 15464 (2007).
9. M. U. Piracha, D. Nguyen, I. Ozdur, and P. J. Delfyett, "Simultaneous ranging and velocimetry of fast moving targets using oppositely chirped pulses from a mode-locked laser," *Opt. Express* **19**, 11213 (2011).
10. S. Darlington, "U.S. Patent No. 2,678,997," (1954).
11. J. R. Klauder, A. C. Price, S. Darlington, and W. J. Albersheim, "The Theory and Design of Chirp Radars," *The Bell Syst. Tech. J.* **39**, 745–808 (1960).
12. A. Chong, J. Buckley, W. Renninger, and F. Wise, "All-normal-dispersion femtosecond fiber laser," *Opt. Express* **14**, 10095–10100 (2006).
13. F. Wise, A. Chong, and W. Renninger, "High-energy femtosecond fiber lasers based on pulse propagation at normal dispersion," *Laser & Photonics Rev.* **2**, 58–73 (2008).
14. Q. Cao, J. Chen, K. Lu, *et al.*, "Sculpturing spatiotemporal wavepackets with chirped pulses," *Photonics Res.* **9**, 2261–2264 (2021).
15. O. Katz, E. Small, Y. Bromberg, and Y. Silberberg, "Focusing and compression of ultrashort pulses through scattering media," *Nat. Photonics* **5**, 372–377 (2011).
16. P. J. Delfyett, D. Mandridis, M. U. Piracha, *et al.*, "Chirped pulse laser sources and applications," *Prog. Quantum Electron.* **36**, 475–540 (2012).
17. C. Hofmann, A. S. Landsman, and U. Keller, "Attoclock revisited on electron tunnelling time," *J. Mod. Opt.* **66**, 1052–1070 (2019).
18. M. A. H. B. M. Yusoff and J. M. Ngoko Djiokap, "Time-delay control of reversible electron spirals using arbitrarily chirped attosecond pulses," *Phys. Rev. A* **109**, 023107 (2024).
19. H. Vincenti and F. Quéré, "Attosecond lighthouses: How to use spatiotemporally coupled light fields to generate isolated attosecond pulses," *Phys. Rev. Lett.* **108**, 113904 (2012).
20. P. E. Hawkins, S. A. Malinovskaya, and V. S. Malinovsky, "Ultrafast geometric control of a single qubit using chirped pulses," *Phys. Scripta* **T147**, 014013 (2012).
21. M. Kuzmanović, I. Björkman, J. J. McCord, *et al.*, "High-fidelity robust qubit control by phase-modulated pulses," *Phys. Rev. Res.* **6**, 013188 (2024).
22. J. O'Sullivan, O. W. Kennedy, K. Debnath, *et al.*, "Random-Access Quantum Memory Using Chirped Pulse Phase Encoding," *Phys. Rev. X* **12**, 041014 (2022).
23. X. Ouyang and J. Zhao, "Orthogonal chirp division multiplexing," *IEEE Trans. on Commun.* **64**, 3946–3957 (2016).
24. X. Li, S. Zhao, G. Wang, and Y. Zhou, "Photonic generation and application of a bandwidth multiplied linearly chirped signal with phase modulation capability," *IEEE Access* **9**, 82618–82629 (2021).
25. S. A. Malinovskaya and V. S. Malinovsky, "Chirped-pulse adiabatic control in coherent anti-Stokes Raman scattering for imaging of biological structure and dynamics," *Opt. Lett.* **32**, 707 (2007).
26. S. Malinovskaya, "Chirped pulse control methods for imaging of biological structure and dynamics," *Int. J. Quantum Chem.* **107**, 3151–3158 (2007).
27. J. Mamou, J. A. Ketterling, and R. H. Silverman, "Chirp-coded excitation imaging with a high-frequency ultrasound annular array," *IEEE Trans. on Ultrason. Ferroelectr. Freq. Control.* **55**, 508–513 (2008).
28. R. D. Niederriter, B. N. Ozbay, G. L. Futia, *et al.*, "Compact diode laser source for multiphoton biological imaging," *Biomed. Opt. Express* **8**, 315–322 (2017).
29. J. F. de Boer, R. Leitgeb, and M. Wojtkowski, "Twenty-five years of optical coherence tomography: the paradigm shift in sensitivity and speed provided by fourier domain oct [invited]," *Biomed. Opt. Express* **8**, 3248–3280 (2017).
30. S. M. Popoff, G. Lerosey, R. Carminati, *et al.*, "Measuring the transmission matrix in optics: An approach to the study and control of light propagation in disordered media," *Phys. Rev. Lett.* **104**, 100601 (2010).

31. L. Chen and S. M. Anlage, "Use of transmission and reflection complex time delays to reveal scattering matrix poles and zeros: Example of the ring graph," *Phys. Rev. E* **105**, 054210 (2022).
32. L. Eisenbud, "The formal properties of nuclear collisions," Ph.D. thesis, Princeton University (1948).
33. E. P. Wigner, "Lower Limit for the Energy Derivative of the Scattering Phase Shift," *Phys. Rev.* **98**, 145–147 (1955).
34. F. T. Smith, "Lifetime Matrix in Collision Theory," *Phys. Rev.* **118**, 349–356 (1960).
35. L. Chen, S. M. Anlage, and Y. V. Fyodorov, "Generalization of wigner time delay to subunitary scattering systems," *Phys. Rev. E* **103**, L050203 (2021).
36. C. G. B. Garrett and D. E. McCumber, "Propagation of a Gaussian Light Pulse through an Anomalous Dispersion Medium," *Phys. Rev. A* **1**, 305–313 (1970).
37. M. D. Crisp, "Concept of Group Velocity in Resonant Pulse Propagation," *Phys. Rev. A* **4**, 2104–2108 (1971).
38. S. Chu and S. Wong, "Linear Pulse Propagation in an Absorbing Medium," *Phys. Rev. Lett.* **48**, 738–741 (1982).
39. R. W. Boyd and D. J. Gauthier, "Slow and fast light," in *Progress in Optics*, E. Wolf Ed., (Elsevier Science, 2002).
40. G. M. Gehring, A. Schweinsberg, C. Barsi, et al., "Observation of Backward Pulse Propagation Through a Medium with a Negative Group Velocity," *Science* **312**, 895–897 (2006).
41. U. Bortolozzo, S. Residori, and J. P. P. Huignard, "Slow and fast light: basic concepts and recent advancements based on nonlinear wave-mixing processes," *Laser & Photonics Rev.* **4**, 483–498 (2010).
42. M. D. Stenner, D. J. Gauthier, and M. A. Neifeld, "The speed of information in a 'fast-light' optical medium," *Nature* **425**, 695–698 (2003).
43. V. A. Sommerfeld, "Concerning the alternating current resistance of coils," *Physikalische Zeitschrift* **8**, 805–809 (1907).
44. L. Brillouin, "Über die fortpflanzung des liches in dispergierenden medien (On the propagation of light in dispersive media)," *Ann. Physik* **44**, 203–240 (1914).
45. L. Brillouin and A. Sommerfeld, *Wave Propagation and Group Velocity* (Academic Press, 1960), chap. 2, pp. 17–39.
46. D. Angulo, K. Thompson, V.-M. Nixon, et al., "Experimental evidence that a photon can spend a negative amount of time in an atom cloud," (2024).
47. K. Thompson, K. Li, D. Angulo, et al., "How much time does a photon spend as an atomic excitation before being transmitted through a cloud of atoms?" *APL Quantum* **2**, 036108 (2025).
48. M. Asano, K. Y. Bliokh, Y. P. Bliokh, et al., "Anomalous time delays and quantum weak measurements in optical micro-resonators," *Nat. Commun.* **7**, 13488 (2016).
49. H. Cao, A. Dogariu, and L. Wang, "Negative group delay and pulse compression in superluminal pulse propagation," *IEEE J. Sel. Top. Quantum Electron.* **9**, 52–58 (2003).
50. D. Waltner and U. Smilansky, "Scattering from a ring graph - a simple model for the study of resonances," *Acta Phys. Polonica A* **124**, 1087–1090 (2013).

Chirped Pulse Analysis and Control in Non-Hermitian Scattering Systems using Complex Time Delay Supplementary Materials

ISABELLA L. GIOVANNELLI,^{1,*} STEVEN M. ANLAGE,¹ AND THOMAS M. ANTONSEN²

¹Quantum Materials Center, Department of Physics University of Maryland, College Park, Maryland 20742, USA

²Department of Electrical and Computer Engineering University of Maryland, College Park, Maryland, 20742, USA

*igiovann@umd.edu

A. Derivation of predictions

A chirped pulse is defined by the following equation in the time domain.

$$E_i(t) \propto \exp \left[-i\omega_0 t - (i\Omega' + \delta_t^{-2}) \frac{t^2}{2} \right] \quad (7)$$

First we Fourier transform this equation into the frequency domain,

$$E_i(\omega) \propto \frac{1}{\sqrt{2\pi}} \int_{-\infty}^{\infty} E_i(t) e^{i\omega t} dt \quad (8)$$

$$\propto \frac{1}{\sqrt{2\pi}} \int_{-\infty}^{\infty} \exp \left[- \left(\frac{i\Omega'}{2} + \frac{1}{2\delta_t^2} \right) t^2 + (-i\omega_0 + i\omega) t \right] dt \quad (9)$$

To evaluate the integral we simply complete the square, leaving us with the following result,

$$E_i(\omega) \propto \exp \left[\frac{-(\omega - \omega_0)^2}{2(i\Omega' + \delta_t^{-2})} \right] \quad (10)$$

To generate the form for the output pulse, we follow the same steps that we did in the Supp. Mat. of Ref. [1]. The highlights will be provided here for convenience. The output pulse will take the form

$$E_o(\omega) \propto \exp[-\kappa + i\phi] E_i(\omega) \quad (11)$$

where $\rho(\omega) = \exp[-\kappa + i\phi]$ is either the transmission or reflection coefficient of a dispersive scattering system, and $\kappa(\omega)$ is the attenuation and $\phi(\omega)$ is the phase shift. Taylor expanding κ and ϕ around center frequency ω_0 we get,

$$\kappa = \kappa(\omega_0) + \left. \frac{d\kappa(\omega)}{d\omega} \right|_{\omega_0} (\omega - \omega_0) + \dots \quad (12)$$

$$\phi = \phi(\omega_c) + \left. \frac{d\phi(\omega)}{d\omega} \right|_{\omega_0} (\omega - \omega_0) + \dots \quad (13)$$

Assuming a pulse frequency bandwidth that is much smaller than the 3dB linewidth of the chosen resonance, we will only use up to the first derivative with respect to frequency, ignoring higher order terms. Using the definition of time delay τ defined in the main text, one can easily find that $\partial\phi/\partial\omega = \text{Re}[\tau]$ and $\partial\kappa/\partial\omega = \text{Im}[\tau]$. Thus,

$$E_o(\omega) \propto E_i(\omega) \exp[(-\text{Im}[\tau] + i\text{Re}[\tau])(\omega - \omega_0)] \quad (14)$$

Separating real and imaginary parts in the exponents,

$$E_o(\omega) \propto \exp\left[\frac{-(\omega - \omega_0)^2}{2(i\Omega' + \delta_t^{-2})}\right] \exp[(-\text{Im}[\tau] + i\text{Re}[\tau])(\omega - \omega_0)] \quad (15)$$

$$\propto \exp\left[\frac{-(\omega - \omega_0)^2(-i\Omega' + \delta_t^{-2})}{2(\Omega'^2 + \delta_t^{-4})}\right] \cdot \exp[-\text{Im}[\tau](\omega - \omega_0)] \cdot \exp[i\text{Re}[\tau](\omega - \omega_0)] \quad (16)$$

$$\propto \exp\left[\frac{-(\omega - \omega_0)^2}{2(\delta_t^2\Omega'^2 + \delta_t^{-2})} - \text{Im}[\tau](\omega - \omega_0)\right] \cdot \exp\left[i\left(\frac{(\omega - \omega_0)^2\Omega'}{2(\Omega'^2 + \delta_t^{-4})} + \text{Re}[\tau](\omega - \omega_0)\right)\right] \quad (17)$$

Now we complete the square in the argument of the red expression, this leaves us with the following,

$$E_o(\omega) \propto \exp\left[-\frac{[(\omega - \omega_0) - (-\tilde{\Delta}^2\text{Im}[\tau])]^2}{2\tilde{\Delta}^2}\right] \exp\left[i\left(\frac{(\omega - \omega_0)^2\Omega'}{2(\Omega'^2 + \delta_t^{-4})} + \text{Re}[\tau](\omega - \omega_0)\right)\right] \quad (18)$$

where $\tilde{\Delta} = \sqrt{\Omega'^2\delta_t^2 + \delta_t^{-2}}$. Note that $\tilde{\Delta}$ is written in terms of Hz in the main text, here we are using angular frequency units. The frequency shift in the magnitude is highlighted in blue.

To find the corresponding time shift, we take the inverse Fourier transform of Eqn. 18,

$$E_o(t) \propto \frac{1}{\sqrt{2\pi}} \int_{-\infty}^{\infty} E_o(\omega) e^{-i\omega t} d\omega \quad (19)$$

This results in the following expression,

$$|E_o(t)| \propto \exp\left[-\frac{((\text{Re}[\tau] - t)\tilde{\Delta} - \tilde{\Delta}^2\text{Im}[\tau]\delta_t\Omega')^2}{2\tilde{\Delta}^2(1 + \delta_t^4\Omega'^2)}\right] \quad (20)$$

$$\propto \exp\left[-\frac{(t - (\text{Re}[\tau] - \text{Im}[\tau]\delta_t^2\Omega'))^2}{2\delta_t^2}\right] \quad (21)$$

where we see that the time shift of the magnitude of the signal is highlighted in blue.

Note that these calculations were done entirely assuming frequency is written as angular frequency. The corresponding variables used in the main text are all written in linear frequency (Hz) to make interpreting the experiment results easier.

B. Derivation of bounds on Ω'

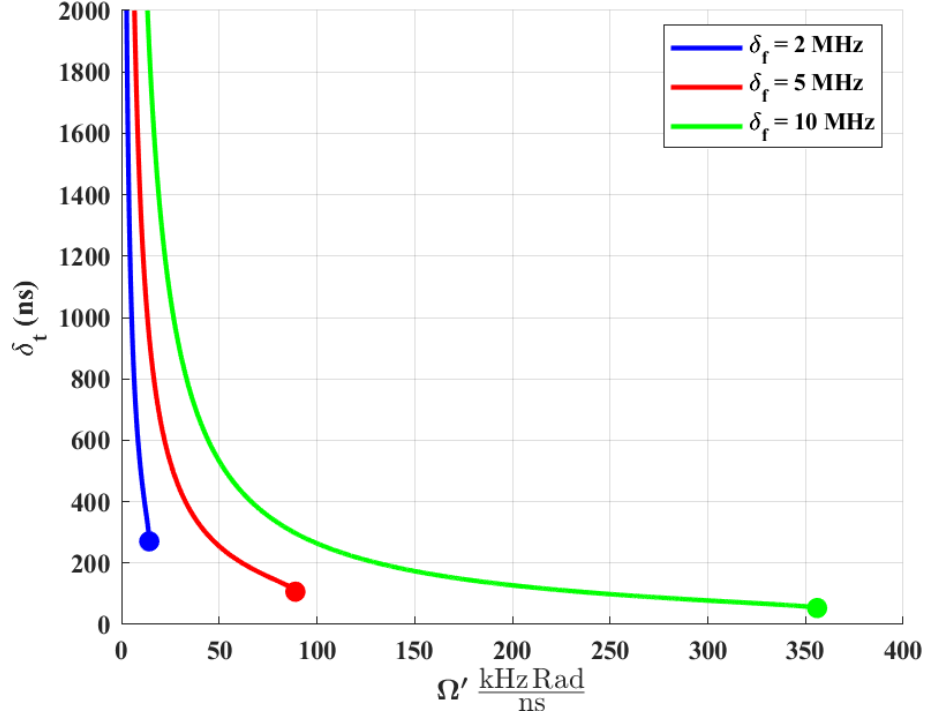


Fig. 6. This is a plot of eqn. 24 versus chirp rate (Ω') for several fixed chirped pulse frequency bandwidth values of 2 MHz (in blue), 5 MHz (in red), and 10 MHz (in green). The end points on each curve correspond to the maximum possible chirp value for a given frequency bandwidth.

The frequency bandwidth of the chirped pulse (in Hz) is defined as,

$$\delta_f = \frac{1}{\pi} \sqrt{2 \ln 2 (\Omega'^2 \delta_t^2 + \delta_t^{-2})} \quad (22)$$

Rearranging this equation we arrive at a quartic polynomial in terms of δ_t ,

$$\Omega'^2 \delta_t^4 - \frac{(\pi \delta_f)^2}{2 \ln 2} \delta_t^2 + 1 = 0 \quad (23)$$

There are 4 roots to this equation. Here we only consider the following root,

$$\delta_t = \sqrt{\frac{\frac{(\pi \delta_f)^2}{2 \ln 2} + \sqrt{\left(\frac{(\pi \delta_f)^2}{2 \ln 2}\right)^2 - 4 \Omega'^2}}{2 \Omega'^2}} \quad (24)$$

Thus, we see that in order for $\delta_t \in \mathbb{R}$ we require,

$$|\Omega'| \leq \frac{(\pi \delta_f)^2}{4 \ln 2} \quad (25)$$

Eqn. 24 is plotted versus chirp rate for various frequency bandwidth values in Fig. 6. Here we see that the maximum chirp rate for a given frequency bandwidth increases with bandwidth as expected from eqn. 25. In general, we see that as Ω' increases, the pulse time width δ_t is bounded below as a result of the constraint on chirp rate (eqn. 25). When $\Omega' \rightarrow 0$ we see that $\delta_t \rightarrow \infty$, so in general the pulse time width can be made arbitrarily large for any finite pulse frequency bandwidth. It is also worth pointing out that there are an infinite number of combinations of δ_t and Ω' that give the same δ_f value. Thus, it is possible to have two chirped pulses with the same frequency bandwidth but with drastically different time shifts (see eqn. 4 in the main text).

C. Additional Data

Figure 7 contains additional chirped pulse reflection data that complements the results shown in Fig. 4 of the main text. Two representative pulses with equal and opposite chirp parameters are illustrated in panels (a) and (b). Figure 8 contains data that is analogous to Fig. 5 in the main text except for the case where the pulse has a frequency bandwidth of 70 MHz (transmission) and 50 MHz (reflection). Figure 9 is the full data set of Fig. 5(b) in the main text. Here we show the multiple divergences for the expected chirp parameter $\Omega' \delta_t^2$ as the imaginary part of reflection time delay crosses through zero.

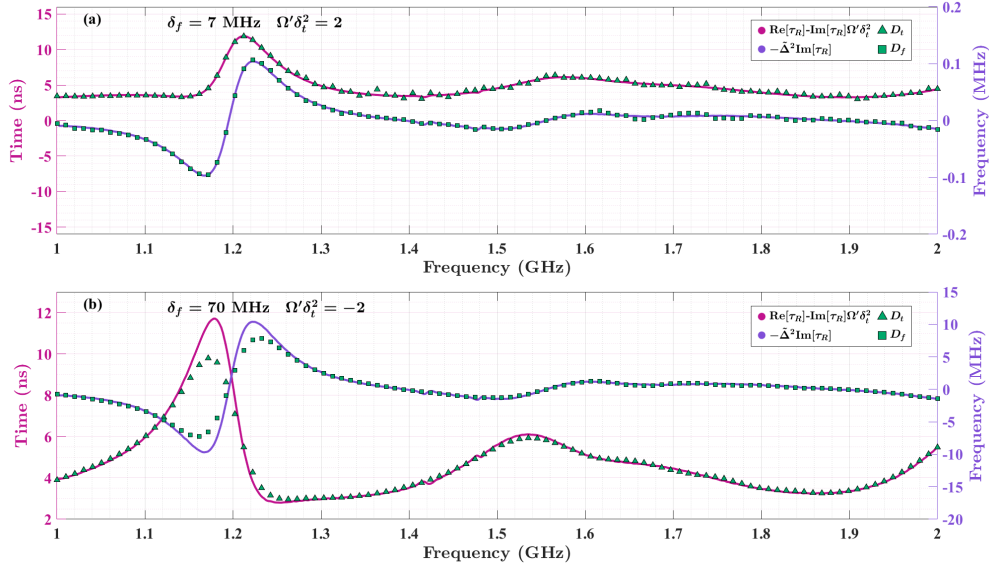


Fig. 7. (a-b) Additional chirped pulse reflection data comparing the predicted center frequency shifts in light purple, and predicted time shifts in magenta with the measured frequency shifts represented as green rectangles and time shifts represented as green triangles. The chirp rates and pulse widths used are as follows: (a) $\Omega' = 0.1395 \frac{\text{MHz Rad}}{\text{ns}}$ and $\delta_t = 119.72$ ns, (b) $\Omega' = -13.9541 \frac{\text{MHz Rad}}{\text{ns}}$ and $\delta_t = 11.97$ ns.

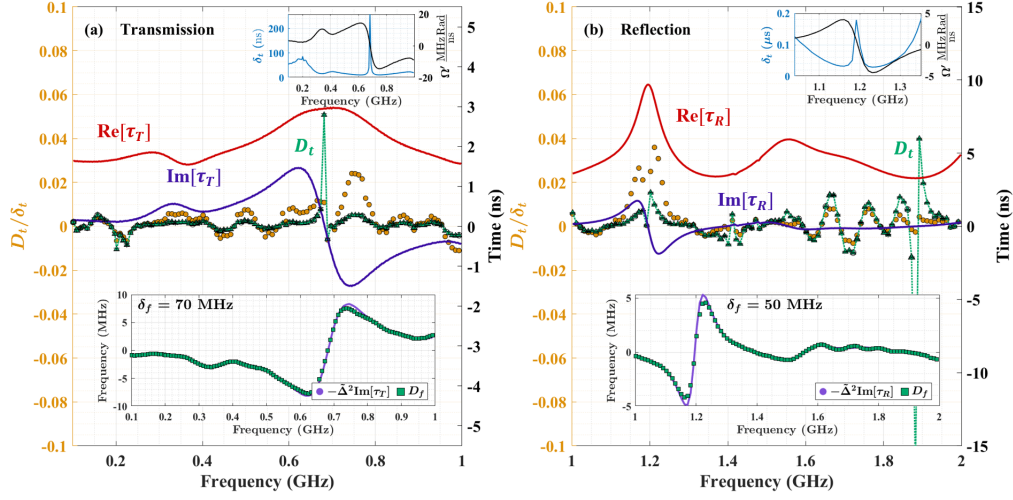


Fig. 8. Additional $D_t = 0$ data where larger frequency bandwidth pulses are used. Panels (a) and (b) are the results for transmission and reflection, respectively. The green triangles correspond to the measured pulse transmission time (right axis). The light orange circles correspond to D_t/δ_t (left axis). The real and imaginary parts of transmission (a) and reflection (b) time delay are plotted in red and dark purple, respectively. The lower insets in (a) and (b) show the predicted and measured pulse frequency shifts plotted in light purple and as green squares respectively. The upper insets show the chosen values of pulse duration δ_t and chirp rate Ω' versus frequency utilized to achieve $D_t = 0$ for the chirped pulse.

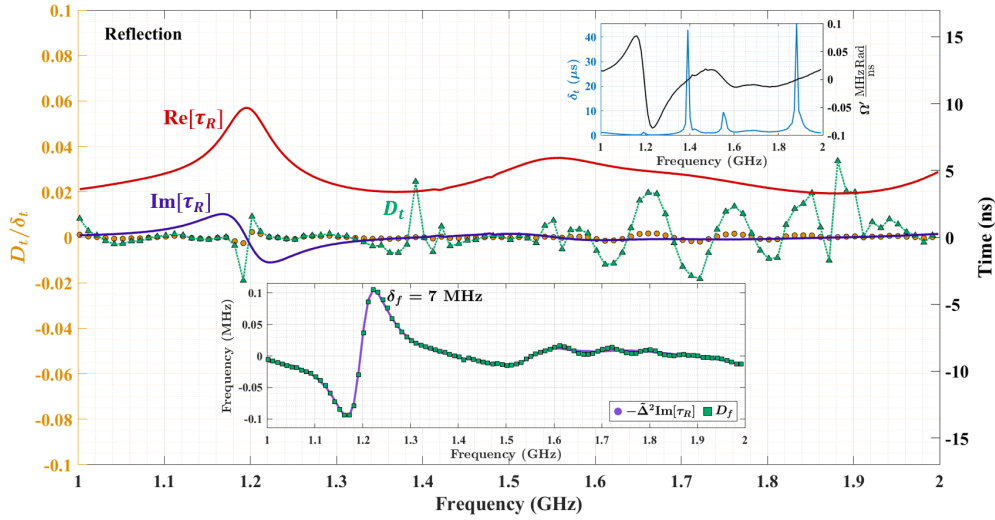


Fig. 9. Additional chirped pulse reflection data showing the full data set of Fig. 5(b) in the main text. The green triangles correspond to the measured pulse transmission time (right axis). The orange circles correspond to D_t/δ_t (left axis). The real and imaginary parts of reflection time delay are plotted in red and dark purple respectively. The lower inset shows the predicted and measured pulse frequency shifts plotted in light purple and as green squares respectively. The upper inset shows the chosen values of δ_t and Ω' versus frequency required to achieve $D_t = 0$ for the chirped pulse.

D. Error Analysis

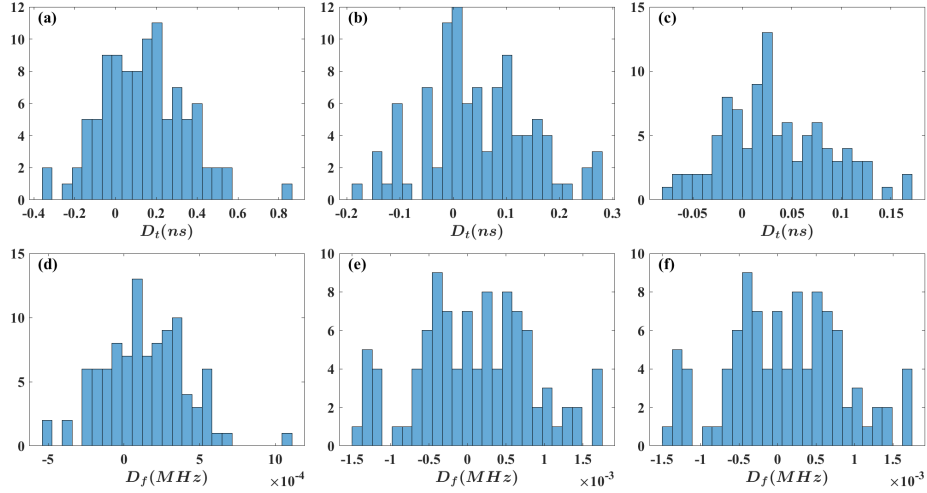


Fig. 10. Time and frequency error analysis for the case where the input pulse has a frequency bandwidth of 5 MHz. Each histogram has 25 bins and 100 data points. The parameters for the plots are as follows: (a),(d) The pulses used have a chirp rate of $\Omega' = 0.008 \frac{\text{MHzRad}}{\text{ns}}$ and a time width of $\delta_t = 1666$ ns. The mean and standard deviation for (a) are 0.13903 ns and 0.2078 ns respectively. For (d) the mean is 0.1384 kHz and the standard deviation is 0.2732 kHz. (b),(e) The pulses have a chirp rate of $0.04 \frac{\text{MHzRad}}{\text{ns}}$ and a time width of 324 ns. The histogram in (b) has a mean of 0.0442 ns and a standard deviation of 0.1001 ns. The analogous histogram (e) has a mean of 92.69 Hz and standard deviation of 0.7642 kHz. Lastly, for (c) and (f) the pulses used have a chirp rate of $0.08 \frac{\text{MHzRad}}{\text{ns}}$ and a time width of 141.41 ns. The mean and standard deviation for (c) are 0.0338 ns and 0.0533 ns respectively. For (f) the mean is 0.1839 kHz and the standard deviation is 0.9306 kHz.

To estimate the measurement statistical error in our experiments we measured a pulse sent through two identical cables. One cable connects Port 1+ on the AWG to channel 1 on the oscilloscope. The other cable connects Port 1- on the AWG to channel 2 on the oscilloscope. The output pulses measured from each cable are then compared by calculating the difference in center frequency and transmission time of the pulse. Ideally, these differences should be zero, however we see in Fig. 10 and Fig. 11 that that is not the case. We tested pulses with various parameters. In Fig. 10 we use pulses that have a frequency bandwidth of 5 MHz and chirp rates ranging from $0.008 \frac{\text{MHzRad}}{\text{ns}}$ to $0.08 \frac{\text{MHzRad}}{\text{ns}}$ with time widths ranging from 141.41 ns to 1666 ns. In Fig. 11 we use pulses that have a frequency bandwidth of 100 MHz and chirp rates ranging from $0.5 \frac{\text{MHzRad}}{\text{ns}}$ to $28.48 \frac{\text{MHzRad}}{\text{ns}}$ with time widths ranging from 8.28 ns to 533.63 ns.

For each case we repeated the measurement 100 times to create the distributions depicted in Figs. 10 and 11. The standard deviations in the shift in frequency are plotted versus chirp rate in Fig. 12(a), and analogously the standard deviations in the shift in time versus the time width of the input pulse is shown in Fig. 12(b). The 5 MHz bandwidth case is plotted in orange and the 100 MHz pulse bandwidth case is plotted in blue. From these plots we clearly see that the standard deviation of D_f increases with chirp rate and the standard deviation of D_t increases with pulse width for both pulse frequency bandwidth cases. In Fig. 12(a) we see that the 100 MHz case consistently has a standard deviation that is larger than the smaller bandwidth case. Conversely, in Fig. 12(b) we see that the 5 MHz case consistently has a larger standard deviation

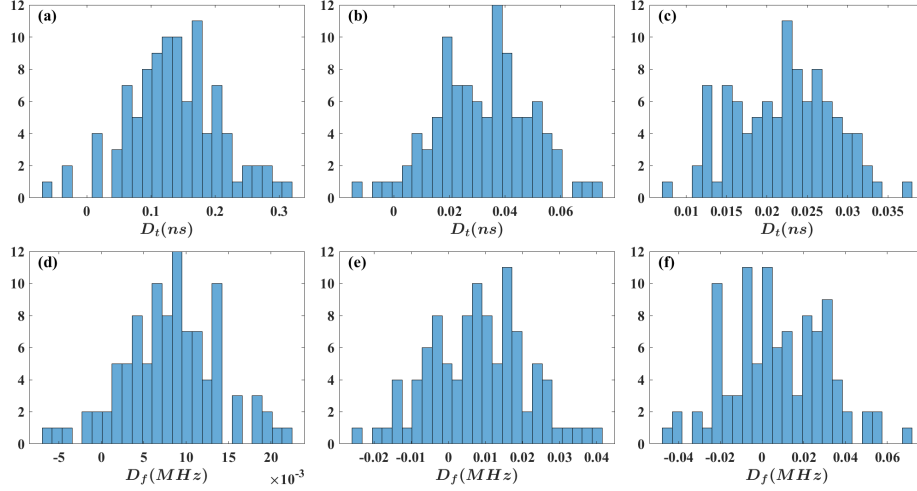


Fig. 11. Time and frequency error analysis for the case where the input pulse has a frequency bandwidth of 100 MHz. Each histogram has 25 bins and 100 data points. The parameters for the plots are as follows: (a)(d) The pulses used have a chirp rate of $\Omega' = 0.5 \frac{\text{MHz Rad}}{\text{ns}}$ and a time width of $\delta_t = 533.63$ ns. The mean and standard deviation for (a) are 0.1360 ns and 0.0713 ns respectively. For (d) the mean is 0.0083 MHz and the standard deviation is 0.0056 MHz. (b)(e) The pulses have a chirp rate of $5 \frac{\text{MHz Rad}}{\text{ns}}$ and a time width of 53.23 ns. The histogram in (b) has a mean of 0.0320 ns and a standard deviation of 0.0170 ns. The analogous histogram (e) has a mean of 0.0079 MHz and standard deviation of 0.013 MHz. Lastly, for (c) and (f) the pulses used have a chirp rate of $28.48 \frac{\text{MHz Rad}}{\text{ns}}$ and a time width of 8.38 ns. The mean and standard deviation for (c) are 0.0221 ns and 0.0060 ns respectively. For (f) the mean is 0.0072 MHz and the standard deviation is 0.0233 MHz.

than the 100 MHz case.

Since the standard deviations for the different bandwidth cases are different, we used different error bars depending on whether the pulse had a bandwidth that is closer to 5 MHz or 100 MHz. Note that the standard deviation in the shift in center frequency is so small that we decided not to include those error bars in our data plots. The error bars on the shift in time measurements are calculated by taking the average of the standard deviations of the corresponding histograms. For the ~ 5 MHz cases we used a value of ± 0.12 ns for the error bars and for the ~ 100 MHz cases we used a value of ± 0.03 ns.

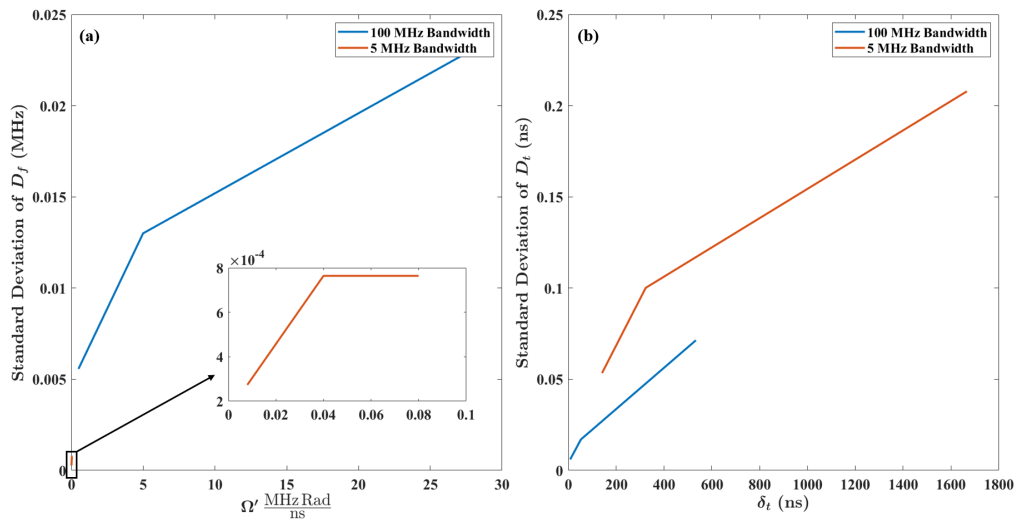


Fig. 12. (a) Standard deviation of the time shift represented by the histograms in (a-c) of Figs. 10 and 11 versus the chirp rate of the input pulse used. The inset is the small boxed region in the lower left zoomed in. (b) Standard deviation of the frequency shift from the histograms in (d-f) of Figs. 10 and 11 versus the time width of the input pulse.